The effect of interbranch spacing on structural and rheological properties of hyperbranched polymer melts

Tu C. Le,[1] B. D. Todd,[1,a)] P. J. Daivis,[2] and A. Uhlherr[3]
[1]*Centre for Molecular Simulation, Swinburne University of Technology, P.O. Box 218, Hawthorn, Victoria 3122, Australia*
[2]*School of Applied Sciences, RMIT University, GPO Box 2476V, Melbourne, Victoria 3001, Australia*
[3]*CSIRO Information Management and Technology, Private Bag 33, Clayton South, Victoria 3169, Australia*

(Received 24 July 2009; accepted 21 September 2009; published online 22 October 2009)

Nonequilibrium molecular dynamics simulations were performed for a family of hyperbranched polymers of the same molecular weight but with different chain lengths between branches. Microscopic structural properties including mean squared radius of gyration, distribution of beads from the center of mass and from the core and the interpenetration function of these systems were characterized. A relationship between the zero shear rate mean squared radius of gyration and the Wiener index was established. The molecular and bond alignment tensors were analyzed to characterize the flow birefringence of these hyperbranched polymers. The melt rheology was also studied and the crossover from the Newtonian to non-Newtonian behavior was captured for all polymer fluids in the considered range of strain rates. Rheological properties including the shear viscosity and normal stress coefficients obtained from constant pressure simulations were found to be the same as those from constant volume simulations except at high strain rates due to shear dilatancy. A linear dependence of zero shear rate viscosities on the number of spacer units was found. The stress optical rule was shown to be valid at low strain rates with the stress optical coefficient of approximately 3.2 independent of the topologies of polymers. © *2009 American Institute of Physics*. [doi:10.1063/1.3247191]

I. INTRODUCTION

In comparison with other classes of materials, polymers have one of the widest ranges of applications such as coatings, additives, drug and gene delivery, macromolecular building blocks, nanotechnology, and supramolecular science.[1] The main key to a large number of applications of polymers is their special properties, which strongly depend on the molecular topologies. Based on the architecture, polymers are classified as linear, branched, or cross-linked polymers. Among these, branched polymers can be further classified as graft, star, comb, or dendritic polymers. The branched polymers that have the most complex architecture are dendritic polymers including dendrimers and hyperbranched polymers. Dendrimers are perfectly branched treelike structures whereas hyperbranched polymers have incompletely or irregularly branched topologies. Therefore, modeling dendrimers is less complicated as the structure is well-defined while simulations of hyperbranched polymers face difficulties as for a given number of monomers, there is a large number of possible architectures of hyperbranched polymers.

As reported in our previous paper,[2] there have been a few papers[3–8] on hyperbranched polymer simulations using Monte Carlo or Brownian dynamics techniques. However only the randomly branched architecture of hyperbranched polymers was modeled and rheological properties of the polymer solution were analyzed. In experiments, although the melts of some hyperbranched polymers have been studied,[9] the architecture of these polymers is also randomly branched due to the difficulties in the synthesis of well-defined dendritic polymers. Recently, dendronized polymers with well-defined structures comprising a linear backbone and attached units of dendrons have been synthesized and modeled[10] but the melt rheology of these systems has not been studied. Therefore our aim in this paper is to study some controlled specific architectures of hyperbranched polymers and the effect of branching topology on the melt rheology. The effect of linear spacers on the rheology of dendritic polymers in solution has been studied experimentally for branched aromatic etherimide copolymers[11] and theoretically for bead-spring-dumbbell model perfectly branched polymers using Brownian dynamics techniques[12] and generalized Gaussian structure—an extension of the Rouse model—for hyperbranched polymers.[13] It has been found that spacer length/number of spacer units is an important architecture parameter that directly affects the rheology of hyperbranched polymer solutions. In this work, nonequilibrium molecular dynamics (NEMD) simulations were performed for a family of hyperbranched polymer melts with the same molecular weight but different numbers of spacer units using coarse-grained[14] uniform beads. The molecular weight of all hyperbranched polymers studied was chosen to be the same as that for perfect trifunctional dendrimers of generation 4. The total number of beads in dendrimers can be calculated as $N_s = fb((f-1)^{g+1}-1)/(f-2)+1$ where f is the functionality of end groups, b is the number of monomers in the chain units, and g is the generation number.[15] With the

a)Electronic mail: btodd@swin.edu.au.

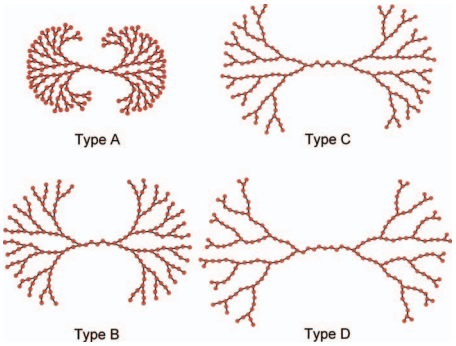

FIG. 1. Schematic architectures of hyperbranched polymers with different numbers of spacers.

choice of $f=3$ and $b=2$, dendrimers of generation 4 will have 187 beads. Structural and rheological properties of this dendrimer as well as a linear chain of equivalent molecular weight were reported previously.[15,16] In order to compare our simulation data with those polymers, different trifunctional ($f=3$) hyperbranched polymers with the same number of beads per molecule were modeled. All polymers have one imperfect branching point with the functionality of end groups $f=2$. Hyperbranched polymers of type A have two beads in the chain units ($b=2$) while polymers of type B, C, and D have three, four, and five beads, respectively, in the chain units. The schematic configuration of these hyperbranched polymers is presented in Fig. 1.

The remainder of this paper is organized as follows. Section II describes the methodology employed consisting of isothermal-isobaric (NpT) and isothermal-isochoric (NVT) NEMD algorithms. Section III A presents the results and a discussion of the structural properties of hyperbranched polymers with different architectures, including mean squared radii of gyration, distribution of mass, and the interpenetration function. Section III B focuses on the flow birefringence effect for these hyperbranched polymers with different spacer lengths. Rheological properties such as the shear viscosity and first and second normal stress coefficients are shown in Sec. III B. Some conclusions are presented in the final section.

II. METHODOLOGY

The models of hyperbranched polymers were built using beads with Weeks–Chandler–Anderson[17] (WCA) intermolecular interaction and finitely extensible nonlinear elastic (FENE) (Ref. 18) bond potential. Nonbonded beads only have the WCA potential interaction, which is the Lennard-Jones potential truncated at the position of the minimum and shifted to eliminate the discontinuity, whereas bonded beads have both FENE and WCA interactions. Details of these potentials can be found in our previous paper.[2] In the remainder of this paper, all quantities are expressed in terms of site reduced units in which the reduction parameters are the Lennard-Jones interaction parameters ε and σ and the mass, $m_{i\alpha}$, of bead α in molecule i. The reduced temperature is given by $T^*=k_BT/\varepsilon$ where k_B is the Boltzmann constant, the density is given by $\rho^*=\rho\sigma^3$, the pressure tensor by $\mathbf{P}^*=\mathbf{P}\sigma^3/\varepsilon$, and strain rate by $\dot{\gamma}^*=(m_{i\alpha}\sigma^2/\varepsilon)^{1/2}\dot{\gamma}$. For simplicity of notation, the asterisk will be omitted hereafter.

To simulate fluids under shear, the molecular version of the SLLOD algorithm[19] was applied. The reasons for using this version of the SLLOD algorithm have been discussed extensively elsewhere.[20] To maintain the constant temperature of simulations, the kinetic energy of the system has been constrained using the molecular version of the Gaussian isokinetic thermostat, which is derived from Gauss's principle of least constraint. The equations of motion for bead α in molecule i are given as

$$\dot{\mathbf{r}}_{i\alpha}=\frac{\mathbf{p}_{i\alpha}}{m_{i\alpha}}+\mathbf{r}_i\cdot\nabla\mathbf{u},$$

$$\dot{\mathbf{p}}_{i\alpha}=\mathbf{F}_{i\alpha}-(m_{i\alpha}/M_i)\mathbf{p}_i\cdot\nabla\mathbf{u}-\zeta(m_{i\alpha}/M_i)\mathbf{p}_i, \quad (1)$$

where $\mathbf{r}_{i\alpha}$ and $\mathbf{p}_{i\alpha}$ represent the position and thermal momentum of bead α in molecule i, $\nabla\mathbf{u}$ is the velocity gradient tensor, $\mathbf{r}_i=\Sigma_{\alpha=1}^{N_\alpha}m_{i\alpha}\mathbf{r}_{i\alpha}/M_i$ is the position of the center of mass of molecule i, $\mathbf{F}_{i\alpha}$ is the intermolecular force on bead α in molecule i, $M_i=\Sigma_{\alpha=1}^{N_\alpha}m_{i\alpha}$ is the mass of molecule i, $\mathbf{p}_i=\Sigma_{\alpha=1}^{N_\alpha}\mathbf{p}_{i\alpha}$ is the momentum of the center of mass of molecule i and $\zeta=\Sigma_{i=1}^{N}\Sigma_{\alpha=1}^{N_s}\mathbf{F}_{i\alpha}\cdot\mathbf{p}_i-\dot{\gamma}\Sigma_{i=1}^{N}p_{ix}p_{iy}/\Sigma_{i=1}^{N}\mathbf{p}_i^2$ is the thermostat constraint multiplier.

All NVT simulations in this work were performed at constant volume at a reduced temperature of 1.25 and the reduced bead density of 0.84.

In order to keep the polymer systems at constant pressure in NpT NEMD simulations, the Nosé–Hoover integral feedback mechanism was implemented.[21] The equations of motion are defined as

$$\dot{\mathbf{r}}_{i\alpha}=\frac{\mathbf{p}_{i\alpha}}{m_{i\alpha}}+\mathbf{r}_i\cdot\nabla\mathbf{u}+\dot{\varepsilon}\mathbf{r}_i,$$

$$\dot{\mathbf{p}}_{i\alpha}=\mathbf{F}_{i\alpha}-(m_{i\alpha}/M_i)\mathbf{p}_i\cdot\nabla\mathbf{u}-\zeta(m_{i\alpha}/M_i)\mathbf{p}_i-\dot{\varepsilon}(m_{i\alpha}/M_i)\mathbf{p}_i, \quad (2)$$

$$\dot{V}=3\dot{\varepsilon}V.$$

The multiplier $\dot{\varepsilon}$ can be obtained by solving the differential equation given by

$$\ddot{\varepsilon}=\frac{(p-p_0)V}{QNk_BT}, \quad (3)$$

where Q is a damping factor, p_0 is the required pressure, and p is the instantaneous isotropic pressure. In this work, Q was chosen to be 1000 to minimize the effect of unphysical oscillations of volume, pressure, or atomic temperature caused by coupling the simulated system to the barostat, hence the melts were allowed to relax to compensate for the flow-induced changes in the pressure. All simulations were performed at the required pressure p_0 of 5.42, which is the equilibrium pressure of the generation 2 dendrimer melt at the density of 0.84 in our previous study.[22]

The equations of motion of the beads were integrated with time step $\Delta t=0.001$ in reduced units using a fifth-order Gear predictor corrector ordinary differential equation solver.[23] After the hyperbranched polymer systems of 125 molecules generated at low density had been compressed to

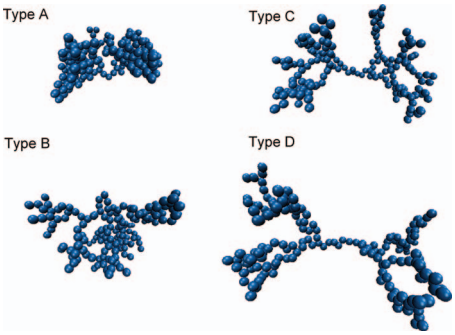

FIG. 2. Typical configurations of simulated hyperbranched polymers composed of 187 beads and different numbers of spacer units: Type A ($b=2$), Type B ($b=3$), Type C ($b=4$), and Type D ($b=5$).

the required density, they were equilibrated for 1×10^6 time-steps and the pressure or density was plotted against time to check if the system had reached the steady state. Twenty separate production simulations, each consisting of 1×10^6 time-steps, are then performed for every system. The means and standard errors were evaluated from results of all the separate runs.

III. RESULTS AND DISCUSSION

A. Structural properties

As stated above, a group of four hyperbranched polymers of the same molecular weight was modeled using coarse-grained uniform beads. Typical instantaneous configurations of these hyperbranched polymers are shown in Fig. 2. As mentioned above, simulated trifunctional hyperbranched polymers have one imperfect branching point with the functionality of end groups $f=2$. They all have the same degree of polymerization N of 187 as for a perfect dendrimer of generation 4. The only difference in their architectures is the number of spacer units. Hyperbranched polymers of type A have the number of spacer units $b=2$ while polymers of type B, C, and D have that of three, four, and five, respectively. Two structural parameters, the degree of branching and the Wiener index, were computed for these systems and results are shown in Table I.

The degree of branching, which is defined as $B=2D/(2D+L)$ where D is the number of fully branched beads and L is the number of partially reacted beads,[24] was calculated for the simulated hyperbranched polymers. The value of the degree of branching varies from 0 for linear polymers to 1 for dendrimers or fully branched hyperbranched polymers. As all simulated systems have only one imperfect branching point, the value of L is always 1. Hyperbranched polymers of type A and B have the same number of fully branched beads of 61, hence they have the same degree of branching of 0.992. Polymers of type C and D have the same number of fully branched beads of 30. Therefore they have the same degree of branching of 0.9836. The same values of the degree of branching for different hyperbranched polymers indicate that the degree of branching only characterizes the extent of unbranched content within a hyperbranched molecule and does not fully describe the architecture of the systems. This is in agreement with many other reports[5–8] on hyperbranched polymers.

TABLE I. Degree of branching and Wiener index for different hyperbranched polymer architectures simulated.

Type of hyperbranched polymers	Degree of branching	Wiener index
A	0.9920	246 388
B	0.9920	306 244
C	0.9836	349 972
D	0.9836	387 540

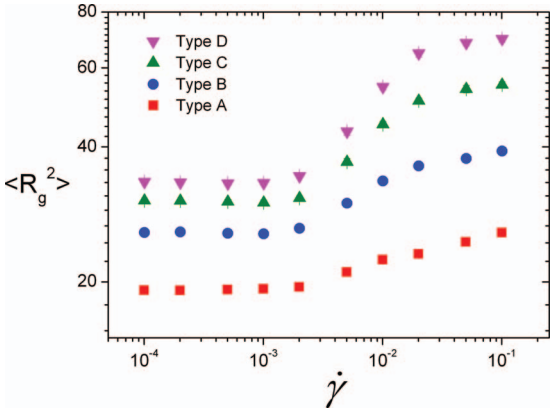

FIG. 3. Dependence of the radius of gyration on strain rate for hyperbranched polymers with different number of spacer units.

In addition to the degree of branching, the Wiener index, defined as $W=1/2\Sigma_{j=1}^{N_s}\Sigma_{i=1}^{N_s}d_{ij}$ where N_s is the number of beads per molecule and d_{ij} is the number of bonds separating bead i and j of the molecule,[6] was calculated to characterize the topologies of simulated hyperbranched polymers in greater detail. This parameter only describes the connectivity and is not a direct measure of the size of the molecules. For polymers of the same molecular weight, linear chain has the largest value of W whereas star polymer with branch length of 1 and the core functionality of N_s-1 has the smallest value of W. In this work, the Wiener index is largest for the type D system, which has the longest linear chain in between branching points (spacer length $b=5$) and smallest for the type A system which has the shortest linear chain between branching points ($b=2$). With increasing number of spacer units from 2 to 5, the values of the Wiener index for hyperbranched polymers comprising 187 beads increase and fall in the range between 246 388 and 387 540. Systems with higher Wiener index or higher number of spacer units have more open structures and larger topological separation of beads.

Figure 3 presents the mean squared radius of gyration, which can be calculated as shown in Eq. (4), for hyperbranched polymers with different spacers,

$$\langle R_g^2\rangle \equiv \left\langle \frac{\Sigma_{\alpha=1}^{N_s} m_\alpha(\mathbf{r}_\alpha-\mathbf{r}_{\mathrm{CM}})\cdot(\mathbf{r}_\alpha-\mathbf{r}_{\mathrm{CM}})}{\Sigma_{\alpha=1}^{N_s} m_\alpha}\right\rangle, \tag{4}$$

where the angular brackets denote an ensemble or time average, $\mathbf{r}_\alpha$ is the position of bead α, and $\mathbf{r}_{\mathrm{CM}}$ is the position of the molecular center of mass. At low strain rates, the value of

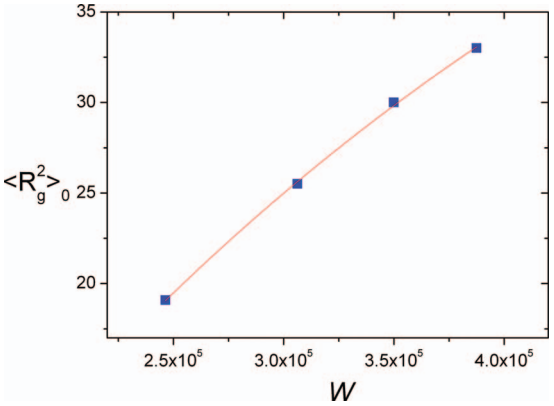

FIG. 4. Dependence of zero shear rate radii of gyration on Wiener index for different hyperbranched polymers of the same molecular weight (the solid line representing fitting with the exponential function).

$\langle R_g^2 \rangle$ remains constant while at high strain rates where molecules are stretched, $\langle R_g^2 \rangle$ increases rapidly. Furthermore as type A molecules have the most dense and rigid structure while type D molecules have the most open and flexible architecture, the radius of gyration rises the least steadily for type A hyperbranched polymers and the most steadily for type D polymers. The ratio of the radii of gyration at strain rates of 0.0001 and 0.1 is 1.34 for type A, 1.52 for type B, 1.81 for type C, and 2.08 for type D polymers. In addition, hyperbranched polymers of type A have the most compact architecture with the least extension of molecules in space as seen from Wiener index, hence at a given strain rate, the radius of gyration is lowest, whereas hyperbranched polymers of type D with the most spatial separation of beads have the highest value of the radius of gyration. Data for the radii of gyration for different hyperbranched polymers were fitted using the Carreau– Yasuda equation[25] $\langle R_g^2 \rangle = \langle R_g^2 \rangle_0 / [1 + (\lambda_{R_g} \dot{\gamma})^2]^{m_{R_g}}$ where $\langle R_g^2 \rangle_0$ is the zero shear rate squared radius of gyration, λ_{R_g} is a time constant, and m_{R_g} is the power law exponent. Results for the zero shear rate radii of gyration were plotted against the Wiener index as shown in Fig. 4. An exponential function gives a very good fit to the zero shear rate mean square radius of gyration. The dependence of $\langle R_g^2 \rangle_0$ on the Wiener index was found to be $\langle R_g^2 \rangle_0 = 65(16) - 87(7) \times e^{-W/(39(16)\times 10^4)}$ where the number in brackets shows the statistical uncertainty from the standard error of the fit. If a power law function is used to fit the $\langle R_g^2 \rangle_0$ data, the zero shear rate mean squared radius of gyration scales as $\langle R_g^2 \rangle_0 \propto W^{1.20(6)}$. The power law exponent of 1.20(6) for these hyperbranched polymers in NEMD simulations is close to the value of 1.0 found for phantom chains neglecting long-range excluded volume interactions and the correction terms in the calculation of the end-to-end distance between two segments.[8] Brownian dynamics simulations[5,6] which take into account the excluded volume and hydrodynamic interactions also showed a power law exponent of approximately 1.0 for hyperbranched polymers of different molecular weights. Specifically the Brownian dynamics results showed that the zero shear rate radius of gyration scales as $\langle R_g \rangle_0 \sim W^{0.5} N_s^{-0.85}$, which means that the squared radius of gyration scales as $\langle R_g^2 \rangle_0 \sim W \times N_s^{-1.7}$. It is interesting that this relationship for hyperbranched polymers is very similar to that for linear chains in good solvents $\langle R_g^2 \rangle_0 \sim W \times N_s^{-1.824}$, which results from $W \sim N_s^3$ for linear polymers and $\langle R_g \rangle_0 \sim N_s^{0.588}$ for linear molecules in good solvents.[26] In ideal solvents or melts, the squared radius of gyration for linear polymers scales as $\langle R_g^2 \rangle_0 \sim N_s$, hence the relationship between W, R_g, and N_s is expected to be $\langle R_g^2 \rangle_0 \sim W \times N_s^{-2.0}$. Taken together these results show that more work is needed to clarify the relationship between W, R_g, and N_s, especially for polymer molecules with short branches.

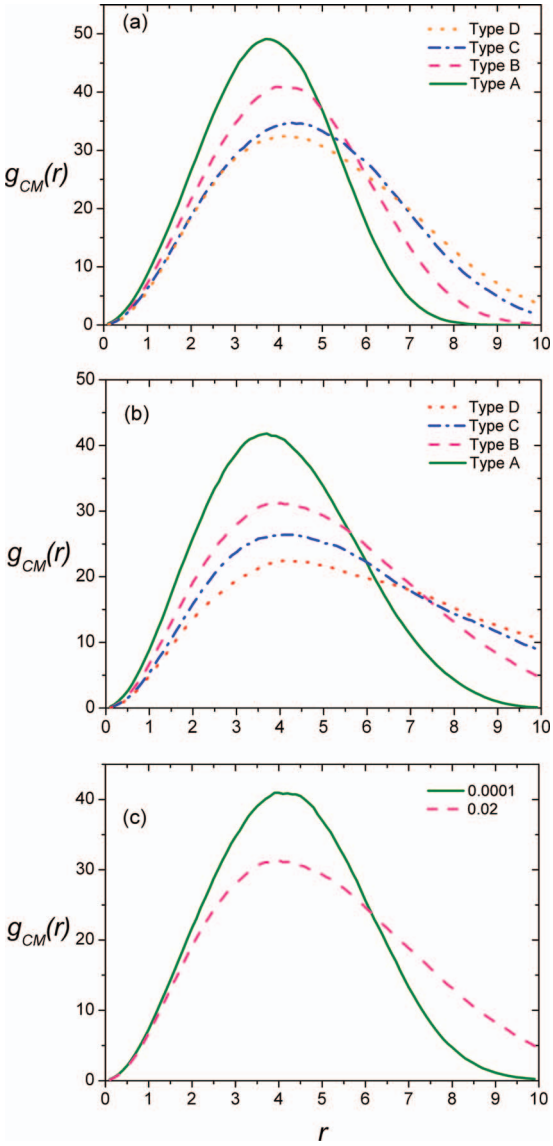

FIG. 5. Distribution of mass from the center of mass for (a) different hyperbranched polymers at strain rate of 0.0001, (b) different hyperbranched polymers at strain rate of 0.02, and (c) hyperbranched polymer of type B at strain rate of 0.0001 and 0.02.

Figure 5 presents the distribution of beads from the molecular center of mass, which is defined as

$$g_{\mathrm{CM}}(r) = \frac{\langle \Sigma_{i=1}^{N} \Sigma_{\alpha=1}^{N_s} \delta(|\mathbf{r} - (\mathbf{r}_{i\alpha} - \mathbf{r}_{\mathrm{CM}})|) \rangle}{N}, \tag{5}$$

where N is the number of molecules, $\mathbf{r}_{i\alpha}$ is the position of bead α in molecule i, and $\mathbf{r}_{\mathrm{CM}}$ is the position of the center of

mass, for hyperbranched polymers of the same molecular weight. With increasing number of spacer units, the distribution of mass becomes broader and the average distance of beads from the center of mass increases. This is in accordance with the topologies of hyperbranched polymer systems simulated. Furthermore the shear-induced behavior of the distribution of mass for different hyperbranched polymers shows a similar trend. At higher strain rates, the curves become wider and the peaks shift toward larger distance as molecules are stretched under shear flow. This behavior was also observed in Brownian dynamics simulations for charged hyperbranched polymers.[4]

In addition to the distribution of beads from the center of mass, another form of intramolecular radial distribution function has been used. The distribution of beads from the central bead (the core), defined as

$$g_{\text{core}}(r) = \frac{\langle \Sigma_{i=1}^{N} \Sigma_{\alpha=2}^{N_s} \delta(|\mathbf{r} - (\mathbf{r}_{i\alpha} - \mathbf{r}_{i1})|) \rangle}{N}, \tag{6}$$

where $\mathbf{r}_{i1}$ is the position of the core, for different hyperbranched polymers is presented in Fig. 6. Strong peaks at the distance equal to the average bond length are observed for all systems corresponding to the first neighbors of the core. The same height of these peaks for different hyperbranched polymers is due to the same number of beads around the core in the innermost shell of the molecules. In contrast, in the outer shells of the molecules, the separation of beads around the core is lowest for the system of type A and highest for the system of type D. Therefore the distribution of beads from the core is the most narrow for type A polymers and broadest for type D polymers. Similar to the radial distribution of beads from the center of mass, the distribution of beads from the core for all hyperbranched polymers under shear flow becomes wider as the molecules are stretched.

In order to characterize the penetration of the volume occupied by the molecule by beads of other molecules, the penetration function, defined as

$$g_{\text{inter}}(r) = \frac{\langle \Sigma_{i=1}^{N} \Sigma_{j\neq i}^{N} \Sigma_{\alpha=1}^{N_s} \delta(|\mathbf{r} - (\mathbf{r}_{j\alpha} - \mathbf{r}_{i1})|) \rangle}{4\pi r^2 N}, \tag{7}$$

where $\mathbf{r}_{i1}$ is the position of the core of molecule i and $\mathbf{r}_{j\alpha}$ is the position of bead α in molecule j, was used and results are shown in Fig. 7. It can be clearly seen that the penetration function for hyperbranched polymers increases with the increase in the number of spacer units. The system of type A has the lowest penetration function while the system of type D has the highest penetration function. This is because polymer molecules with longer linear chains between branching points are more open and freely accessible by beads of other molecules whereas polymers with short chains between branching points have more compact structures, which reduce the probability of finding parts of other molecules in the interior of a polymer molecule. Furthermore, under shear flow, the interpenetration increases with the increase in strain rate as molecules are stretched and become more open, hence parts of other molecules can gain access closer to the core of the hyperbranched polymer molecule.

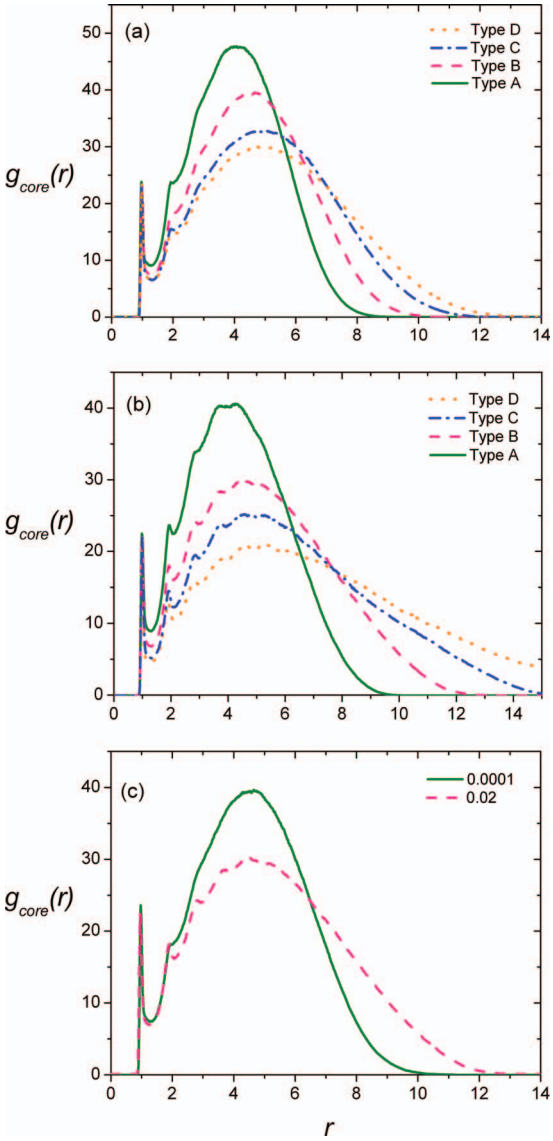

FIG. 6. Distribution of mass from the core for (a) different hyperbranched polymers at strain rate of 0.0001, (b) different hyperbranched polymers at strain rate of 0.02, and (c) hyperbranched polymer of type B at strain rate of 0.0001 and 0.02.

B. Flow birefringence

In order to characterize the flow birefringence effect for hyperbranched polymer structures, the molecular and bond alignment tensors were computed. The form birefringence is the birefringence caused by the alignment of the whole molecules. This can be characterized by the molecular alignment tensor defined as $\mathbf{S}_m = \langle \Sigma_{i=1}^{N} (\mathbf{u}_i \mathbf{u}_i - 1/3\mathbf{I}) \rangle$, where N is the total number of molecules, $\mathbf{u}_i$ is the unit vector denoting the orientation of single molecules, and $\mathbf{I}$ is the unit tensor. On the other hand, the intrinsic birefringence is the birefringence due to the alignment of intramolecular bonds, which can be characterized by the bond alignment tensor defined as $\mathbf{S}_b = \langle \Sigma_{i=1}^{N} \Sigma_{\alpha=1}^{N_s-1} (\mathbf{u}_{i\alpha} \mathbf{u}_{i\alpha} - 1/3\mathbf{I}) \rangle$ where $\mathbf{u}_{i\alpha}$ is the unit vector between adjacent beads.

Figure 8 shows the molecular alignment angle, χ_m, and the bond alignment angle, χ_b, for different hyperbranched polymers. The molecular alignment angle is the average

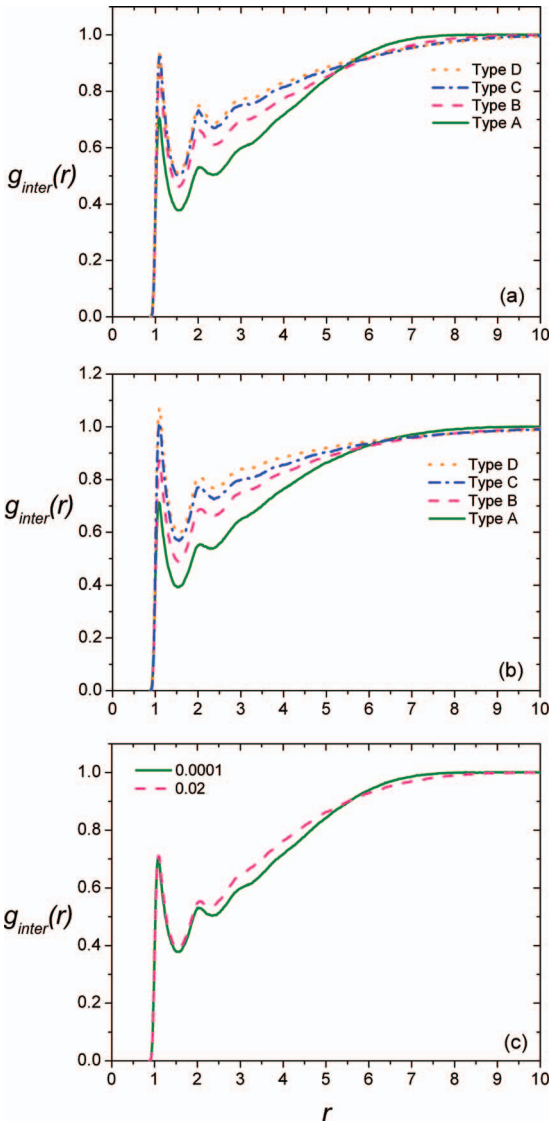

FIG. 7. Comparison of the interpenetration function for (a) different hyperbranched polymers at strain rate of 0.0001, (b) different hyperbranched polymers at strain rate of 0.02, and (c) hyperbranched polymer of type A at strain rate of 0.0001 and 0.02.

angle between the flow direction and the molecular alignment direction. On the other hand, the bond alignment angle is the average angle between the flow direction and the bond alignment direction. At low strain rates where polymer systems are in the Newtonian regime, both molecular and bond alignment angles reach 45°. At high strain rates where systems are in the non-Newtonian regime, the hyperbranched polymer of type A has the highest values of the alignment angles χ_m and χ_b while the polymer of type D has the lowest values of χ_m and χ_b. This again can be explained by the topologies of these systems. Type A hyperbranched polymer with the smallest number of spacer units has the most compact and constrained structure. With increasing number of spacer units, polymer architectures become less rigid, hence molecules and bonds can stretch and align more easily with respect to the flow field. Furthermore, at high strain rates, the bond alignment angle is always higher than the molecular alignment angle of the same polymer type.

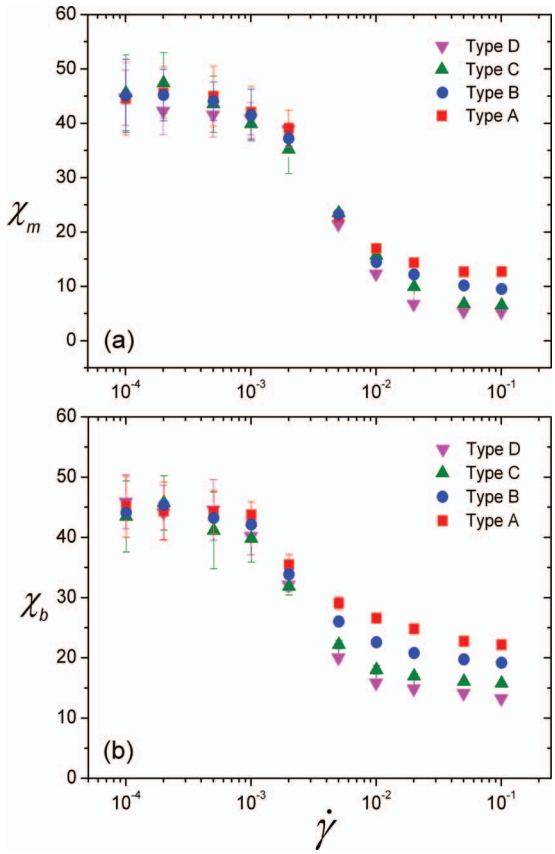

FIG. 8. (a) Molecular and (b) bond alignment angle for different hyperbranched polymers at different strain rates.

Figure 9 presents the molecular order parameter S_m, defined as 3/2 of the largest eigenvalue of the molecular alignment tensor and the bond order parameter S_b, defined as 3/2 of the largest eigenvalue of the bond alignment tensor. The other eigenvalues of the alignment tensor are about half of the largest eigenvalues indicating weaker ordering in the other two directions. Such ordering is consistent with the prolate ellipsoid molecular shape characterized by the eigenvalues of the gyration tensor as discussed in our previous paper.[2] The order parameter of the molecular alignment tensor is actually a measure of the ordering of the anisotropy of the directors of the molecules. In all cases, the order parameter remains constant at low strain rates and increases in high strain rate regions. This indicates that for all hyperbranched polymers, the orientational ordering increases and the alignments of molecules and bonds are more pronounced at high strain rates. It can also be seen that with increasing number of spacer units, the order parameter increases. The order parameter for hyperbranched polymers with smaller number of spacer units is always lower than that for polymers with larger number of spacer units. This is because they have more compact and constrained structures and it is more difficult for the chain segments to stretch and align with respect to the flow field. Furthermore the bond order parameter is always much lower than the molecular order parameter. This is due to the high level of branching of hyperbranched polymers and the excluded volume effect. In addition, the small-scale features are always less distorted by shear.[27]

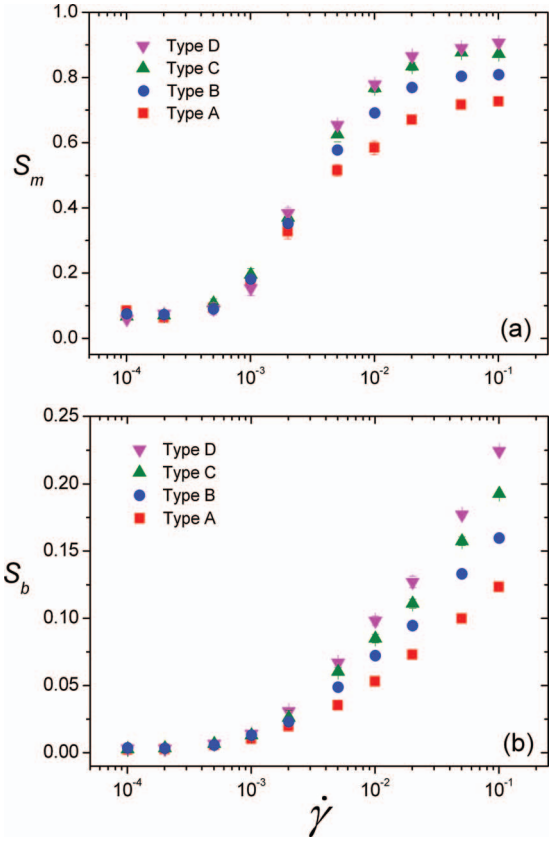

FIG. 9. Order parameter of the (a) molecular and (b) bond alignment tensors for different hyperbranched polymers at different strain rates.

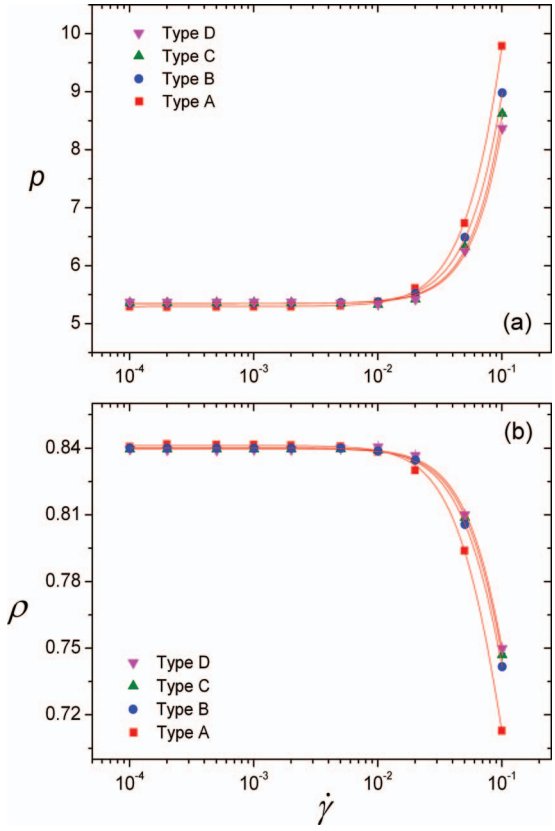

FIG. 10. Dependence of the (a) isotropic pressure and (b) reduced bead density on strain rate of different hyperbranched polymers in NVT and NpT simulations, respectively (solid lines representing fitting with the Carreau–Yasuda model).

C. Rheological properties

The rheological properties of the polymer fluids under shear flow can be calculated from the components of the molecular pressure tensor,[20] which is given by

$$\mathbf{P}^M V = \left\langle \sum_{i=1}^{N} \frac{\mathbf{p}_i \mathbf{p}_i}{M_i} - \frac{1}{2} \sum_{i=1}^{N} \sum_{\alpha=1}^{N_s} \sum_{j \neq i}^{N} \sum_{\beta=1}^{N_s} \mathbf{r}_{ij} \mathbf{F}_{i\alpha j\beta} \right\rangle, \tag{8}$$

where $\mathbf{p}_i$ is the total peculiar center of mass momentum of molecule i, as defined by the equations of motion, $\mathbf{r}_{ij}=\mathbf{r}_j-\mathbf{r}_i$ is the center of mass separation of molecules i and j, $\mathbf{F}_{i\alpha j\beta}$ is the intermolecular force on bead α in molecule i due to bead β in molecule j.

The isotropic pressure of polymeric systems under shear can be calculated as

$$p = \tfrac{1}{3} Tr(\mathbf{P}^M) = \tfrac{1}{3}(P_{xx} + P_{yy} + P_{zz}). \tag{9}$$

Results of the isotropic pressure for different hyperbranched polymers in NVT simulations are shown in Fig. 10(a). It can be seen that at low strain rates, the pressure of all systems reaches a plateau while at high strain rates, the pressure increases rapidly. This indicates that the behavior of the isotropic pressure moves from the Newtonian to non-Newtonian regime. In comparison to linear and other branched polymers, the pressure for hyperbranched polymers shows a different trend. A drop can be observed in the plot of pressure versus strain rate for linear, star, H, and comb-shaped polymer melts comprising of $C_{100}H_{202}$ molecules.[28] Before the rapid increase in pressure, linear molecules exhibit a pressure drop of about 5% while the pressure of other branched polymers only have a small drop. The pressure data for hyperbranched polymers were fitted using the Carreau– Yasuda equation $p=p_0/[1+(\lambda_p\dot{\gamma})^2]^{m_p}$ where p_0 is the zero shear rate pressure, λ_p is a time constant from and m_p is the power law exponent. Fitting parameters are shown in Table II. As can be seen from this table, the zero shear rate isotropic pressure slightly increases with increasing number of spacer units due to the larger spatial separation of beads. Furthermore, the critical strain rate $\dot{\gamma}_{\text{critical}}$ at which the transition from Newtonian to non-Newtonian behavior of the pressure occurs can be calculated as the inverse of λ_p. The values of $\dot{\gamma}_{\text{critical}}$ were found to be 0.06(2), 0.07(3), 0.09(2), and 0.09(2) for hyperbranched polymers with the number of spacer units of 2, 3, 4, and 5, respectively.

TABLE II. Parameters of the Carreau–Yasuda model fitted to the isotropic pressure vs strain rate dependence for NVT simulations.

Type of hyperbranched polymers	p_0	λ_p	m_p
A	5.295(6)	16.9(7)	−0.46(2)
B	5.334(4)	14.1(7)	−0.48(3)
C	5.336(9)	11(2)	−0.6(1)
D	5.34(1)	11(3)	−0.6(3)

TABLE III. Parameters of the Carreau–Yasuda model fitted to the reduced bead density vs strain rate dependence for NPT simulations.

Type of hyperbranched polymers	ρ_0	λ_ρ	m_ρ
A	0.8412(2)	12.6(5)	0.175(9)
B	0.8400(1)	11.1(3)	0.156(6)
C	0.8400(2)	9.4(8)	0.18(2)
D	0.8400(4)	9(2)	0.21(9)

In contrast to NVT simulations with constant density and changing pressure, NpT simulations have constant pressure and variable density. Figure 10(b) shows the reduced bead density as a function of shear rate in constant pressure simulations. It can be seen that the density reaches a plateau at low strain rates while at high strain rates, the density falls rapidly. This phenomenon is called shear dilatancy.[29] Density data are fitted using the Carreau–Yasuda equation $\rho=\rho_0/[1+(\lambda_\rho\dot{\gamma})^2]^{m_\rho}$ where ρ_0 is the zero shear rate density, λ_ρ is a time constant, and m_ρ is the power law exponent. Results for these parameters are presented in Table III. The time constant for density λ_ρ has lower values than that for isotropic pressure λ_p. Therefore the critical strain rates at which the transition from Newtonian to non-Newtonian behavior of the reduced bead density occurs are higher than those for the pressure.

From the components P_{xy} and P_{yx} of the molecular pressure tensor $\mathbf{P}^M$, the non-Newtonian shear viscosity of hyperbranched polymer fluids can be calculated as $\eta=-\langle P_{xy}+P_{yx}\rangle/2\dot{\gamma}$. Shear viscosity data at different strain rates obtained from NpT and NVT simulations are presented in Fig. 11. As can be seen, the shear thinning behavior is captured within the considered range of strain rates for hyperbranched polymers of all types. The viscosities reach a plateau at low strain rates then decrease rapidly at high strain rates. Furthermore, the viscosities of the simulated fluids increase with increasing number of spacer units. Hyperbranched polymers of type A possess the lowest shear viscosities whereas polymers of type D have the highest viscosities. This is because hyperbranched polymers with a larger number of spacer units have longer branches and more open structure, which lead to more entanglement in the systems and result in higher values of viscosity. However, at very high strain rates, the trend is reversed, hyperbranched polymers with longer spacer length have lower viscosities than those with shorter spacer length. Results obtained from NVT and NpT simulations only differ from each other at high strain rates as they then apply to different state points. Viscosity values in the high strain rate regions obtained from constant pressure simulations are lower than those from constant volume simulations. The reason for the more pronounced shear thinning behavior in NpT simulations is because of the "shear dilatancy"—the density decreases as the shear rate increases. However NpT and NVT simulation results will be the same if the same state point is investigated by setting the required pressure in NpT simulations equal to the pressure obtained from NVT simulations at a given strain rate.[21]

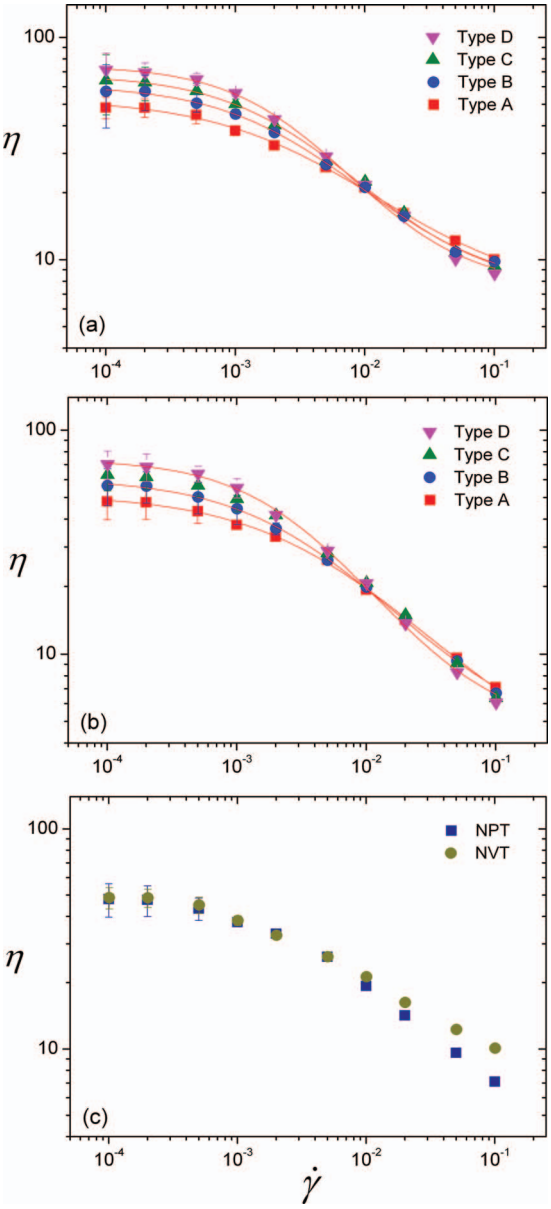

FIG. 11. Shear viscosities vs strain rate for (a) different hyperbranched polymers in NVT simulations, (b) different hyperbranched polymers in NpT simulations, and (c) hyperbranched polymer of type A in NVT and NpT simulations (solid lines representing fitting with the Cross model).

Viscosity data were fitted using the Cross equation[30] which is given by $\eta=\eta_\infty+(\eta_0-\eta_\infty)/(1+(K\dot{\gamma})^{m_C})$ where η_0 is the zero shear viscosity, η_∞ is the infinite shear viscosity, K is the consistency index, and m_C is the power law index. Fitting parameters are shown in Table IV. The NpT simulation zero shear rate viscosities obtained from the Cross equation fit are then plotted against the number of spacer units and results are shown in Fig. 12. It can be clearly seen that zero shear rate viscosities correlate linearly with the number of spacer units b in hyperbranched polymer systems simulated. The slope of the line is found to be 7.3(2). The linear dependence of η_0 on the number of spacer units has also been investigated in Brownian dynamics simulations[12] for hyperbranched polymers comprising 66 beads per molecule and in experiments[11] for hyperbranched aromatic etherimide copolymers.

TABLE IV. Parameters of the Cross model fitted to the shear viscosity vs strain rate dependence.

Type of hyperbranched polymers	NVT				NpT			
	η_∞	η_0	K	m	η_∞	η_0	K	m
A	7(2)	53(2)	322(46)	0.74(9)	3(2)	52(1)	241(24)	0.72(7)
B	7(1)	61(1)	374(28)	0.86(6)	4(1)	60(1)	336(25)	0.81(6)
C	7(1)	67(1)	391(30)	0.90(7)	3(1)	67(1)	347(21)	0.82(5)
D	8(2)	74(2)	408(30)	1.01(8)	5(1)	74(2)	380(30)	0.96(8)

Viscosity data were also fitted using the Carreau–Yasuda equation in the form $\eta=\eta_0/[1+(\lambda_\eta\dot{\gamma})^2]^{m_\eta}$ where λ_η is a time constant and m_η is the power law exponent. The fitting parameters for all simulated hyperbranched polymer systems are presented in Table V. The inverse of the time constant λ_η is the strain rate $\dot{\gamma}_{\text{critical}}$ at which the onset of shear thinning is observed. As the values of λ_η increase with increasing number of spacer units, the critical strain rate $\dot{\gamma}_{\text{critical}}$ is lowest for hyperbranched polymer of type A with the lowest Wiener index and highest for polymer of type D with the largest Wiener index. A similar behavior of the critical strain rate was found for hyperbranched polymers under elongational flow in Brownian simulations.[5] Furthermore the time constant in the Carreau–Yasuda model fitted to the shear viscosity data from NpT simulations is always lower than that from NVT simulations. Therefore the value of the critical strain rate for a given hyperbranched polymer system at constant pressure is always higher than that at constant volume. As mentioned above, NVT and NpT algorithms will give the same results if the same state point is investigated.

The time constant λ_η in the Carreau–Yasuda model fitted to the viscosity data is also the longest relaxation time τ_0 of molecules composing the fluids from which the Weissenberg number We can be calculated by the definition $We=\dot{\gamma}\tau_0$. As shown in our previous paper,[31] using the Weissenberg number, a master curve can be established and the shear rate dependence of the viscosity for hyperbranched polymers of different molecular weights in the same series could be predicted. With the same purpose, the ratios of shear viscosity and zero shear rate viscosity for hyperbranched polymers of four different architectures are plotted against the Weissenberg number. However results show that using the Weissenberg number calculated from the time constant in the Careau–Yasuda model and normalized viscosity is not sufficient to eliminate differences between different architectures. Therefore the time constant in the Cross model is used to compute the Weissenberg number and viscosity data were normalized using different parameters in the Cross models. Although this gives a better result in eliminating the differences between simulated architectures, a master curve still cannot be established as shown in Fig. 13.

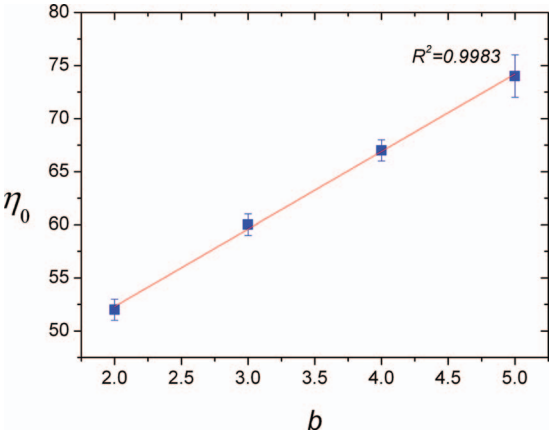

FIG. 12. Dependence of zero shear rate viscosities on the number of spacer units for hyperbranched polymers.

From the components of the molecular pressure tensor $\mathbf{P}^M$, the first and second normal stress coefficients, which describe the effect of the normal stress differences exhibited by polymeric fluids, can be calculated by the definitions $\psi_1=\langle P_{yy}-P_{xx}\rangle/\dot{\gamma}^2$ and $\psi_2=\langle P_{zz}-P_{yy}\rangle/\dot{\gamma}^2$. Results for ψ_1 and $-\psi_2$ for hyperbranched polymers with different number of spacer units are shown in Figs. 14 and 15. It can be seen that the first and second normal stress coefficients are always higher for systems with longer branches. However, the gap between the values of the normal stress coefficients of different hyperbranched polymers is more pronounced for ψ_1 than that for $-\psi_2$. The crossover from Newtonian to non-Newtonian behavior cannot be captured due to the noise of data in the low strain rate region. The normal stress coefficients for all simulated hyperbranched polymers in NpT and NVT simulations were fitted in the power-law region. The exponents α and β of the asymptotic dependences $\psi_1\propto\dot{\gamma}^{-\alpha}$ and $|\psi_2|\propto\dot{\gamma}^{-\beta}$ are presented in Table VI. Similar to the behavior of the shear viscosity, the rate of decrease in the normal stress coefficients is more pronounced for NpT simulations, hence the exponents α and β obtained from NpT simulations have higher values than those from NVT simulations. However, these values are still within the range of typical experimental values for polymer melts and concentrated solutions.[25]

Figure 16 shows the deviations from the stress optical rule (SOR) which can be tested using the components of the molecular pressure tensor P_{xx}, P_{yy}, and P_{zz} together with components of the bond alignment tensor S_{xx}, S_{yy}, and S_{zz}. As can be seen, components of the stress and alignment tensors are proportional, hence the SOR is valid, only in the low strain rate region. The proportionality constant—the stress optical coefficient—is independent of the number of spacer units and has the value of approximately 3.2, which is very close to the obtained stress optical coefficient for hyperbranched polymers type A at different molecular weight. This is in agreement with experimental results which show that the stress optical coefficient does not depend on the molecu-

TABLE V. Parameters of the Carreau–Yasuda model fitted to the shear viscosity vs strain rate dependence.

Type of hyperbranched polymers	NVT			NpT		
	η_0	λ_η	m_η	η_0	λ_η	m_η
A	48(6)	1422(615)	0.158(2)	47(1)	1338(240)	0.18(1)
B	57.5(4)	1524(87)	0.186(4)	56.0(7)	1471(137)	0.200(8)
C	63(5)	1612(93)	0.195(5)	62.2(7)	1562(127)	0.214(8)
D	75(19)	1918(1268)	0.214(9)	69.6(5)	1801(730)	0.245(7)

lar weight or branching of molecules.[26] As discussed in our previous paper,[2] the violation of the SOR in the high strain rate region occurs because it does not take into account the flow-induced changes of the radial distribution function of hyperbranched polymers that becomes distorted at high strain rates. Furthermore the deviations from the SOR correspond to the point where the pressure $p(\dot{\gamma})$, which depends on the radial distribution function, begins to vary rapidly as can be seen in Fig. 10(a) rather than that for the shear viscosity $\eta(\dot{\gamma})$ as seen in Fig. 11. This confirms that the deviations are due to the changes in the local structure.

IV. CONCLUSIONS

In this work, hyperbranched polymers of the same molecular weight of 187 beads but with different number of spacer units of 2, 3, 4, and 5 were modeled using NEMD. The degree of branching was found to possess the same value for polymers of type A and B as well as for polymers of type C and D. Therefore the Wiener index W was calculated to fully characterize the architecture of simulated systems. Microscopic structural properties, flow birefringence, and melt rheology of these systems were found to change significantly with an increasing number of spacer units.

The radius of gyration, distribution of beads, and the interpenetration function were in accordance with the mo-

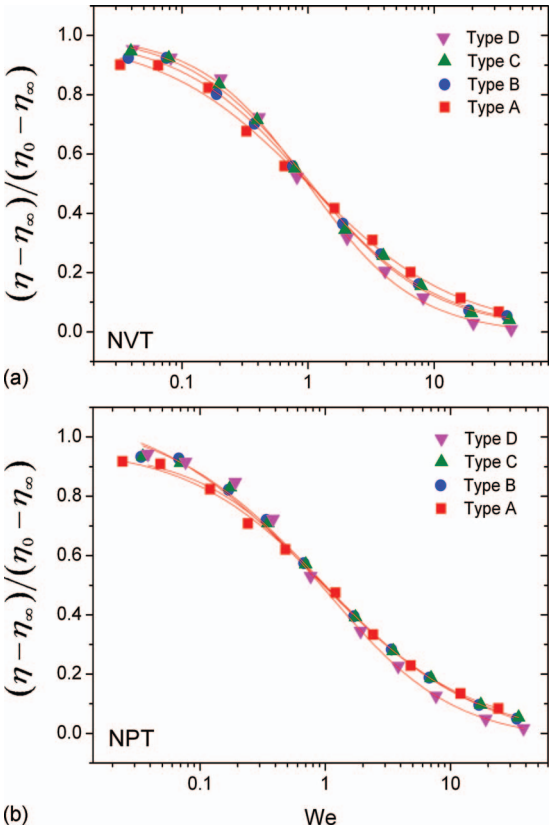

FIG. 13. Shear viscosities vs Weissenberg number for different hyperbranched polymers in (a) NVT and (b) NpT simulations (solid lines representing fitting with the Cross model).

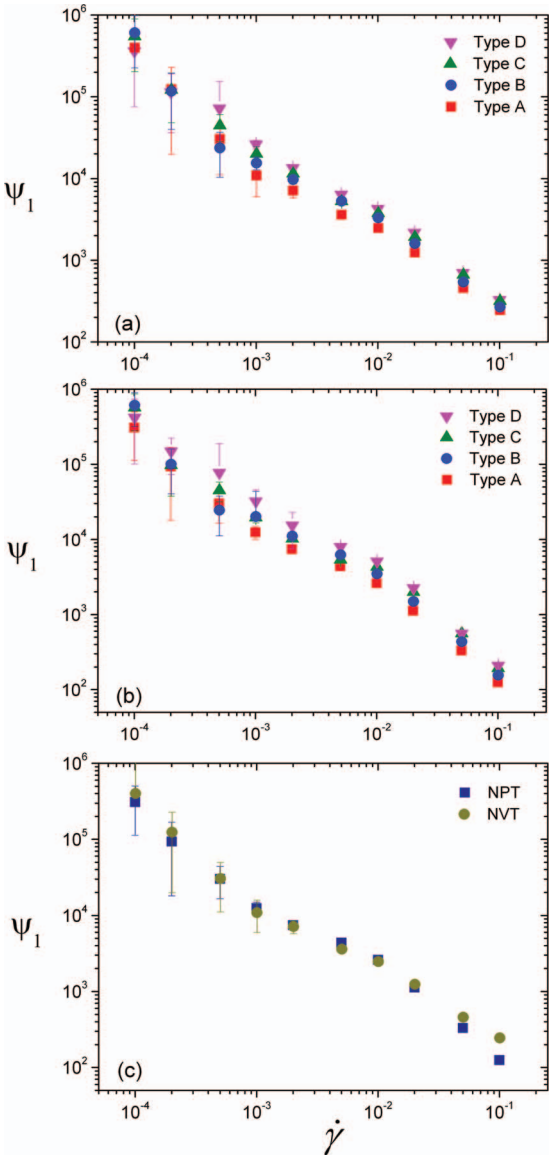

FIG. 14. First normal stress coefficient vs strain rate for (a) different hyperbranched polymers in NVT simulations, (b) different hyperbranched polymers in NpT simulation, and (c) hyperbranched polymer of type A in NVT and NpT simulations.

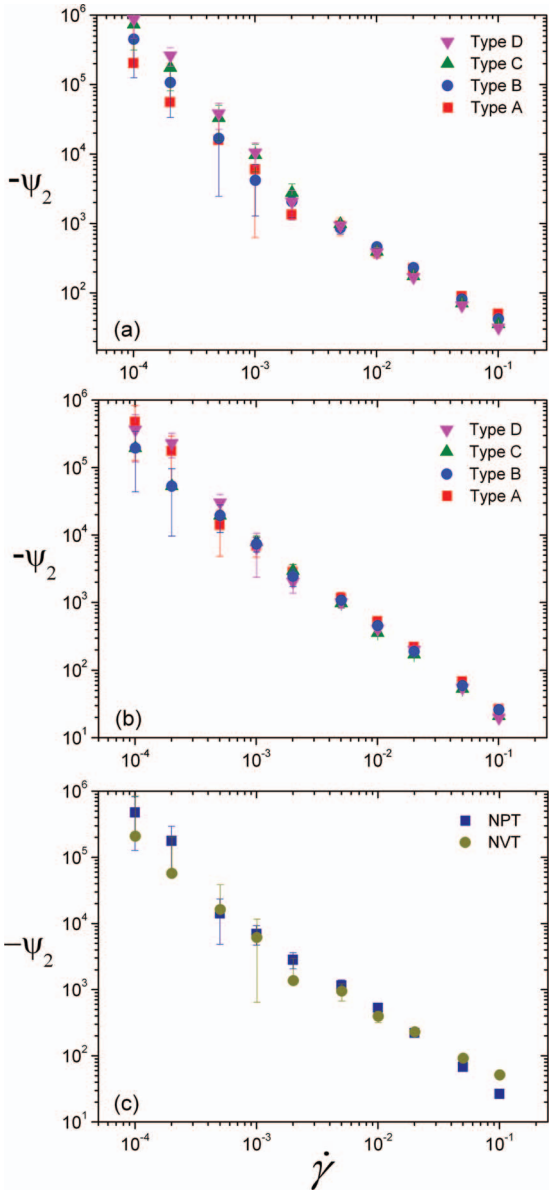

FIG. 15. Second normal stress coefficient vs strain rate for (a) different hyperbranched polymers in NVT simulations, (b) different hyperbranched polymers in NpT simulations, and (c) hyperbranched polymer of type A in NVT and NpT simulations.

lecular architecture being less compact and more open with an increasing number of spacer units and have significant changes induced by the shear flow. The mean squared zero shear rate radius of gyration was found to scale with the Wiener index as $\langle R_g^2 \rangle_0 \propto W^{1.20(6)}$.

TABLE VI. Estimated values of the exponents in the power law regions for the first and second normal stress coefficients of different hyperbranched polymers.

Type of hyperbranched polymers	NVT		NpT	
	α	β	α	β
Type A	1.0(2)	0.9(7)	1.2(5)	1.27(4)
Type B	1.1(1)	1.0(3)	1.2(6)	1.26(9)
Type C	1.0(9)	1.1(1)	1.1(9)	1.1(3)
Type D	1.1(5)	1.1(4)	1.2(6)	1.1(6)

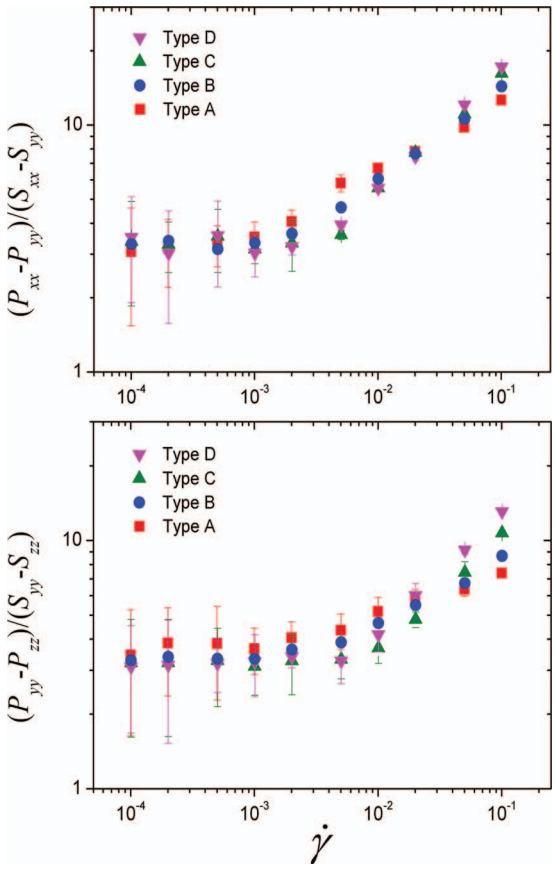

FIG. 16. Deviations from the stress optical rule—$(P_{xx}-P_{yy})/(S_{xx}-S_{yy})$ and $(P_{yy}-P_{zz})/(S_{yy}-S_{zz})$ vs the logarithm of $\dot{\gamma}$ for different hyperbranched polymers.

For all systems, the flow alignment angle always converges to 45° in the Newtonian regime and decreases in the non-Newtonian regime. Furthermore the molecular alignment angle is found to be lower than the bond alignment angle. On the other hand, the order parameter for simulated hyperbranched polymers remains constant in the low strain rate region and increases at high strain rates. Besides, the smaller value of the bond alignment parameter in comparison with the molecular alignment parameter indicates that the intrinsic birefringence is fairly small compared to the form birefringence.

The crossover from the Newtonian to non-Newtonian behavior was captured for all polymeric fluids in the range of strain rates considered. Rheological properties obtained from NpT simulations were found to be the same as those from NVT simulations except at high strain rates due to shear dilantancy. A linear dependence of zero shear rate viscosities on the number of spacer units was found for the hyperbranched polymer systems simulated. Furthermore it has been found that using the Weissenberg number and normalized viscosity is not sufficient to eliminate differences between different architectures of hyperbranched polymers. Although the isotropic pressure in NVT simulations and reduced bead density in NpT simulations show opposite trends, they both have large critical strain rate at which the transition from the Newtonian to non-Newtonian behavior occurs. Furthermore the SOR was shown to be valid at low

strain rates with the stress optical coefficient of approximately 3.2 independent of the polymer topologies.

[1] C. Gao and D. Yan, Prog. Polym. Sci. **29**, 183 (2004).
[2] T. C. Le, B. D. Todd, P. J. Daivis, and A. Uhlherr, J. Chem. Phys. **130**, 074901 (2009).
[3] D. Konkolewicz, O. Thorn-Seshold, and A. Gray-Weale, J. Chem. Phys. **129**, (2008).
[4] G. K. Dalakoglou, K. Karatasos, S. V. Lyulin, and A. V. Lyulin, J. Chem. Phys. **129**, 034901 (2008).
[5] I. M. Neelov and D. B. Adolf, J. Phys. Chem. B **108**, 7627 (2004).
[6] P. F. Sheridan, D. B. Adolf, A. V. Lyulin, I. Neelov, and G. R. Davies, J. Chem. Phys. **117**, 7802 (2002).
[7] A. V. Lyulin, D. B. Adolf, and G. R. Davies, Macromolecules **34**, 3783 (2001).
[8] A. H. Widmann and G. R. Davies, Comput. Theor. Polym. Sci. **8**, 191 (1998).
[9] S. Kunamaneni, D. M. A. Buzza, D. Parker, and W. J. Feast, J. Mater. Chem. **13**, 2749 (2003); Suneel, D. M. A. Buzza, D. J. Groves, T. C. B. McLeish, D. Parker, A. J. Keeney, and W. J. Feast, Macromolecules **35**, 9605 (2002); S. B. Kharchenko, R. M. Kannan, J. J. Cernohous, S. Venkataramani, and G. N. Babu, J. Polym. Sci., Part B: Polym. Phys. **39**, 2562 (2001); T. T. Hsieh, C. Tiu, and G. P. Simon, Polymer **42**, 7635 (2001); T. T. Hsieh, C. Tiu, and G. P. Simon, *ibid.* **42**, 1931 (2001); P. J. Farrington, C. J. Hawker, J. M. J. Frechet, and M. E. Mackay, Macromolecules **31**, 5043 (1998).
[10] Y. Guo, J. D. Van Beek, B. Zhang, M. Colussi, P. Walde, A. Zhang, M. Kroger, A. Halperin, and A. D. Schluter, J. Am. Chem. Soc. **131**, 11841 (2009); Y. Ding, H. C. Ottinger, A. D. Schluter, and M. Kroger, J. Chem. Phys. **127**, 094904 (2007).
[11] L. J. Markoski, J. S. Moore, I. Sendijarevic, and A. J. McHugh, Macromolecules **34**, 2695 (2001).
[12] A. T. Lee and A. J. McHugh, Macromolecules **34**, 7127 (2001).
[13] C. Satmarel, C. Von Ferber, and A. Blumen, J. Chem. Phys. **124**, (2006).
[14] C. N. Likos, Soft Matter **2**, 478 (2006).
[15] J. T. Bosko, B. D. Todd, and R. J. Sadus, J. Chem. Phys. **121**, 1091 (2004).
[16] J. T. Bosko, B. D. Todd, and R. J. Sadus, J. Chem. Phys. **121**, 12050 (2004); **124**, 044910 (2006).
[17] J. D. Weeks, D. Chandler, and H. C. Anderson, J. Chem. Phys. **54**, 5237 (1971).
[18] G. S. Grest and K. Kremer, Phys. Rev. A **33**, 3628 (1986).
[19] D. J. Evans and G. P. Morriss, *Statistical Mechanics of Nonequilibrium Liquids* (Academic, London, 1990).
[20] B. D. Todd and P. J. Daivis, Mol. Simul. **33**, 189 (2007).
[21] P. J. Daivis and D. J. Evans, J. Chem. Phys. **100**, 541 (1994).
[22] J. T. Bosko, B. D. Todd, and R. J. Sadus, J. Chem. Phys. **123**, (2005).
[23] C. W. Gear, *Numerical Initial Value Problems in Ordinary Differential Equations* (Prentice-Hall, Englewood Cliffs, NY, 1971).
[24] D. Holter, A. Burgath, and H. Frey, Acta Polym. **48**, 30 (1997).
[25] R. B. Bird, C. F. Curtiss, R. C. Armstrong, and O. Hassager, *Dynamics of Polymeric Liquids* (Wiley, New York, 1987).
[26] M. Doi and S. F. Edwards, *The Theory of Polymer Dynamics* (Clarendon, Oxford, 1986).
[27] M. Kroger, W. Loose, and S. Hess, J. Rheol. **37**, 1057 (1993).
[28] A. Jabbarzadeh, J. D. Atkinson, and R. I. Tanner, Macromolecules **36**, 5020 (2003).
[29] O. Reynolds, Philos. Mag. **20**, 469 (1985).
[30] M. M. Cross, J. Colloid Sci. **20**, 417 (1965).
[31] T. C. Le, B. D. Todd, P. J. Daivis, and A. Uhlherr, J. Chem. Phys. **131**, 044902 (2009).